# Microscopic and bulk properties of symmetric nuclear and pure neutron matter with chiral $N^3LO$ nucleon-nucleon force

Kh.S.A. Hassaneen[1&2], H.M. Abou-Elsebaa[1], E.A.Sultan[1] and N.N. Abd Allah[1]
Physics department, Faculty of Science, Sohag University, Sohag, Egypt.
Physics department, Faculty of Science, Taif University, Taif, Saudi Arabia

**Abstract**— We have studied the single-particle properties and the equation of state (EOS) of symmetric nuclear and neutron matter within the framework of the Brueckner-Hartree-Fock (BHF) approach extended by including a phenomenological three-body force (3BF). Adding the 3BF to the initial two-body force (2BF) and applying a partial-wave expansion, *G*-matrix calculations are performed in pure neutron matter as well as in symmetric nuclear matter. The 3BF is shown to affect significantly the nuclear matter EOS at high densities above the normal nuclear matter density and it is necessary for reproducing the empirical saturation property of symmetric nuclear matter in a non-relativistic microscopic framework. The calculations have been done using the charge-dependent chiral nucleon-nucleon interaction at order four $N^3LO$ potential and compared with both the CD-Bonn and Argonne $V_{18}$ potentials plus the three-nucleon Urbana interaction. It is found that the calculations with the $N^3LO$ potential alone for symmetric nuclear matter at high density is strongly over bound in the BHF approximation.

**Index Terms**—Chiral Force, Equation of State, Partial Waves, Pure Nuclear Matter, Symmetric Nuclear Matter, Three-Body Force.



## 1 INTRODUCTION

The study of microscopic and bulk properties of infinite nuclear matter starting from realistic models of two-body forces (2BF) is still one of the challenging open problems in nuclear physics. In fact, the presence of strong short-range and tensor components in the realistic 2BF, which are required to fit the deuteron properties and nucleon-nucleon (NN) scattering data, are the origin of the corresponding correlations in the nuclear wave function. The study of these correlations and their influence on different observables has made important progress not only from the theoretical side but also from the experimental point of view [1]. The short-range correlations and the nucleon momentum distribution in nuclear matter have been examined by using different approaches, such as the Brueckner-Hartree-Fock (BHF) [2], variational [3, 4], Monte Carlo technique [5, 6], self-consistent Green's function method [7, 8], etc. The only input required in these calculations is the realistic NN interaction.

Actually all the results for the nuclear equation of state (EOS) using various microscopic calculations with only realistic 2BF fail to reproduce the exact saturation point extracted from the phenomenological data on a wide set of nuclei. Different two-body interactions give in general different saturation points, all outside the phenomenological constraints. In particular within the Brueckner theory, with the standard choice of the single particle potential, the theoretical saturation points appear to lie along the celebrated "Coester band" [9]. If the so-called "continuous choice" is adopted, the Coester band seems to coalesce within in a more limited region of the energy-density plane, but still the phenomenological region is missed [10]. There are various attempts have been made to include other methods to improve the description of the saturation properties. One way is, three-body forces (3BF) have been widely used to implement the nuclear Hamiltonian and to shift the saturation point towards the phenomenological one [11]. There is another method such as relativistic effects and 3BF contributions in the nuclear medium. It was demonstrated that relativistic Brueckner-Hartree-Fock calculations [12] can provide a satisfactory saturation curve. However, because contributions from higher-order correlations and three-nucleon forces have not been fully estimated in the relativistic treatment, the problem seems not to be settled yet.

In the present work, three different 2BFs are chosen, with very different short-range and tensor components, to explore the widest possible range. The alteration of the results with the underlying 2BF provides an indication of the validity of the physical effects at play. The first of them is the Idaho next-to-next-to-next-to-leading-order ($N^3LO$) chiral-perturbation-theory potential of Ref. [13]. Its low-energy constants are fitted to reproduce the two-body scattering data with a large accuracy in a $\chi 2$ procedure [14]. Owing to its very nature, as an effective-field-theory potential, the interaction requires a momentum cutoff, which is chosen at 500MeV. In general, this 2BF induces relatively few high-momentum components in the many-body wave function. This is particularly true beyond the cutoff momentum, where the potential is not expected to apply. The second one is the charge-dependent Bonn (CD-Bonn) interaction is based on a meson-exchange picture and provides a very accurate fit to the two-body scattering data

[15]. Its short-range core is soft, which yields less high-momentum components. Also, we use the Argonne (V18) contains a π-exchange plus parameterizations in real space, including 18 spin-isospin operators [16]. It is local and a typical example of a particularly strong, but finite, short-range core. All these 2BFs are phase-shift equivalent.

Kohno [17] has calculated EOS of symmetric nuclear matter and pure neutron matter, using the N$^3$LO interaction and NNLO 3BF of the Jülich group [18]. In the chiral effective field theory, the 3BF is introduced in a systematic way along with the NN potential. Three of the five coupling constants in the NNLO 3BF are fixed in a NN sector. The remaining two parameters are under control in the literature in terms of reproducing the properties of few-nucleon systems. The 3BF is treated by reducing it to density-dependent NN interactions by folding single-nucleon degrees of freedom in infinite matter. His calculated results show that the empirical saturation property is well reproduced in nuclear matter. In the present work, the N$^3$LO NN potentials complemented by phenomenological Urbana 3BFs [19], instead of chiral three-nucleon forces, have been applied in calculations to nuclear and neutron matter.

We will calculate the ground-state properties of infinite symmetric nuclear matter within the framework of Brueckner-Hartree-Fock theory using three different 2BFs. The effects of the 3BF are taken into account via a density-dependent two-body potential, phenomenological Urbana type that is added to the chiral N$^3$LO potential 2BF.

## 2 FORMALISM

The basic ingredient in BHF approach is the reaction matrix G, which satisfies the following Bethe-Goldstone equation:

$$G(\omega,\rho) = V + \sum_{k_a k_b} V \frac{|k_a k_b\rangle Q \langle k_a k_b|}{\omega - e(k_a) - e(k_b) + i\eta} G(\omega,\rho), \quad (1)$$

Where V is the bare realistic 2N interaction, ρ is the nuclear matter density, ω is the starting energy, and Q is Pauli operator which restricts the intermediate states to particle states with momenta ka, kb, which are above the corresponding Fermi momentum. The single-particle energy e(k) which is used in equation (1) can be interpreted as the physical energy of a particle (hole) at momentum k inside nuclear matter, i.e. the quasi-particle energy in the language of the many-body theory. e (k) is a simple sum of kinetic and potential energies U(k) and has the form:

$$e(k) = T + U(k) = \frac{\hbar^2 k^2}{2m} + U(k) \quad (2)$$

Then U(k) can be interpreted as the single-particle optical potential in nuclear matter. This interpretation requires that U(k) is continuous at k=$k_F$. This choice of the auxiliary potential has been advocated by Mahaux and his group [20]. In general, U(k) can be adopted to be the self energy Σ(k, e(k)) of the nucleon with momentum k. Therefore, if one adopts the continuous choice for the auxiliary potential, then U(k) can be written as,

$$U(k,\rho) = Re \sum_{k' \le k_F} \langle k k' | G(e(k) + e(k')) | k k' \rangle_a \quad (3)$$

for all values of |k|. Once the single-particle potential is calculated, one can easily calculate the binding energy per nucleon for symmetric nuclear matter of density $\rho = 2(k_F)^3/(3\pi^2)$: $k_F$ is the Fermi momentum of SNM,

$$\frac{E(k)}{A} = \frac{3}{5}\frac{k_F^2}{2m} + \frac{1}{2\rho} Re \sum_{k' \le k_F} \langle k k' | G(e(k) + e(k')) | k k' \rangle_a \quad (4)$$

where the suffix a denotes antisummarization. The matrix elements of G can be used to evaluate the partial waves contributions to the total energy per nucleon. In the case of the exact Pauli operator this energy is given as [21]

$$\frac{E}{A} = \frac{3}{10}\frac{k_F^2}{m} + \frac{6}{k_F^3} \sum_{\substack{T,S,M,l',\lambda, \\ J',J,m_l,m_s}} (2T + 1) \int k^2 dk \int K^2 dK \int d\Omega \times \langle klJ | G_{STM}(\omega,K) | kl'J' \rangle (l' m_l S m_s | J' M)(l m_l S m_s | JM) Y_{l'm_l}(\Omega) Y_{lm_l}(\Omega) \times \Theta\left(k_F - \left|\vec{K} + \vec{k}\right|\right)\Theta\left(k_F - \left|\vec{K} - \vec{k}\right|\right) \quad (5)$$

with Ω being the angle between the direction of the relative momentum k and the center-of-mass momentum K. In the calculations discussed below we consider the coupling of partial waves up to Jmax, Jmax ≤ 9.

In the present work, the phenomenological Urbana interaction [19] has been adopted to study the effect of 3BFs on the EOS. It consists of an attractive term due to two-pion exchange with excitation of an intermediate Δ resonance, and a repulsive phenomenological central term. The suggested 3BF is reduced to a density dependent two-body force by averaging on the position of the third particle, assuming that the probability of having two particles at a given distance is reduced according to the two-body correlation function. Explicitly, the 3BF is written as [22]

$$V_{ijk} = V_{ijk}^{2\pi} + V_{ijk}^{R} \quad (6)$$

The first one is the so-called Fujita-Miyazawa two-pion exchange contribution. It is a cyclic sum over the nucleon indices i, j, k of products of anticommutator {,} and commutator [,] terms

$$V_{ijk}^{2\pi} = A\sum_{cyc}\left(\{X_{ij},X_{jk}\}\{\tau_i,\tau_j,\tau_j,\tau_k\} + \frac{1}{4}[X_{ij},X_{jk}][\tau_i,\tau_j,\tau_j,\tau_k]\right) \quad (7)$$

Where

$$X_{ij} = Y(r_{ij})\sigma_i.\sigma_j + T(r_{ij}).S_{ij} \quad (8)$$

is the one-pion exchange operator, σ and τ are known as the Pauli spin and isospin operators, and
$S_{ij} = 3\left[(\sigma_i.r_{ij})(\sigma_j.r_{ij}) - \sigma_i.\sigma_j\right]$
is called the tensor operator. Both Y(r) and T(r) are the Yukawa and tensor functions associated to the one-pion exchange as in the 2B potential. The repulsive term is written as

$$V_{ijk}^{R} = U\sum_{cyc} T^2(r_{ij}).T^2(r_{jk}) \quad (9)$$

The strengths A and U are parameters that in the present work are adjusted to reproduce the exact saturation point of symmetric nuclear matter.

## 3 Results and Discussion

### 3.1 The single-particle potential

In Fig. 1 the results for nuclear and neutron matter obtained in microscopic many-body calculations – BHF without three-body forces using three-different 2BFs are shown together with three-body forces. The single-particle potential as function of momentum is illustrated at the empirical value of saturation density $\rho_0$ = 0.16 fm-3 various models for the NN interactions. These models are, with high accuracy fits to the NN scattering data, N$^3$LO potential [13] which is based on chiral perturbation theory, CD-Bonn [15] and Argonne $V_{18}$ [16] potentials. In the case of symmetric nuclear matter and without 3BF contributions, the single-particle potential is more attractive using N$^3$LO potential displayed with solid line than CD-Bonn with dash line and Argonne $V_{18}$ with dash-double dotted curve interactions. Also, the single particle potentials are equal to -93.9, -91.9 and -87.7 MeV at k = 0 for the N$^3$LO, CD-Bonn and Argonne V18 interactions, respectively, in the case of BHF approximation only. This means that the effective interaction is more attractive between nucleons in the case of N$^3$LO potential. There is another indication for the differences between the interactions considered: the Argonne $V_{18}$ is local and is stiffer than the N$^3$LO and CD-Bonn that are nonlocal interaction. Therefore a larger part of the attraction in the effective interaction originates from the particle-particle ladder contributions to the G-matrix. This is true in particular for the proton-neutron interaction, which can be traced back to the correlations in the $^3S_1$-$^3D_1$ channel of the interacting nucleons with total iso-spin T = 0 [1].
When 3BF is complemented to the effective two-body force, the situation is different, especially for the N$^3$LO displayed by dotted curve and CD-Bonn with dash-dotted line potentials. One observes that the single-particle potential becomes less attractive than introduced by BHF approach. Also the depth of it has the values -90.01 and -86.77 MeV for N$^3$LO and CD-Bonn potentials, respectively. On the contrary, with the Argonne $V_{18}$ with 3BF, one observes only very slight quantitative changes and the corresponding plots are not shown. This may be because of its strongly repulsive core. There is another behavior of single-particle potentials which show a significant deviation from a parabolic shape in particular at momentum slightly above the Fermi momentum $k_F$ [10, 23]. It is obvious that such a deviation tends to provide more attractive matrix elements of G-matrix in evaluating the self-energy for hole states according to equation 3, which leads to more binding energy.

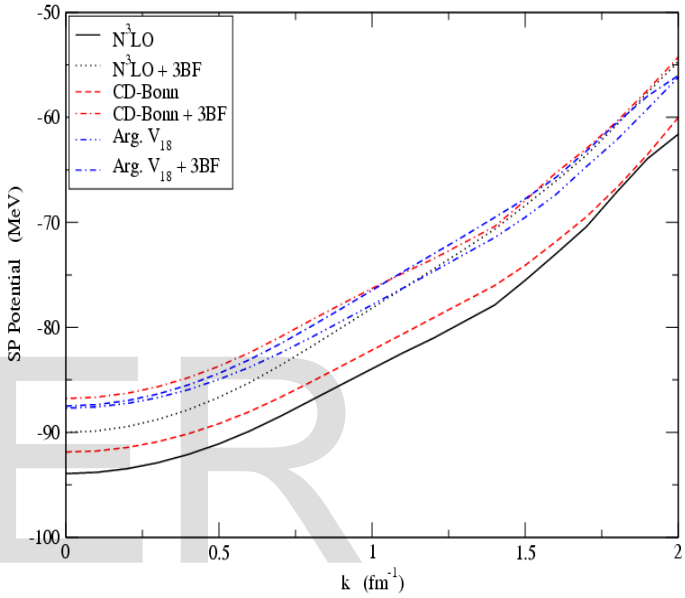


Fig. 1. The single-particle potential as a function of momentum. The calculations are done for symmetric nuclear matter with a Fermi momentum $k_F$ = 1.35 fm$^{-1}$ using chiral N$^3$LO, CD-Bonn and Argonne $V_{18}$ potentials with and without 3BF in the frame of the BHF approach.

### 3.2 EOS of symmetric nuclear and pure neutron matter

In Fig. 2, we display our BHF results with and without 3BF of the EOS for SNM. In the case of BHF only, the solid line denotes the results from the only two-body chiral potential N$^3$LO, which compared with both dashed line by CD-Bonn and dash-double dotted line with Argonne $V_{18}$ potentials. The empirical estimates of the binding energy are shown as the rectangular box in Fig. 2, whereas the solid points indicate the saturation points of each interaction. These three forces give EOS which differs substantially between each other. In particular, for N$^3$LO potential the saturation point falls at the Fermi momentum $k_F \approx$ 1.90 fm$^{-1}$ with an energy per particle $E/A \approx$ -26.22 MeV, this extremely high saturation density is

remedied by the 2NF in the BHF approach. For the CD Bonn the saturation point lies at the Fermi momentum $k_F \approx 1.7$ fm$^{-1}$ with an energy per particle $E/A \approx -22.51$ MeV, while for $V_{18}$ the saturation point is $k_F \approx 1.50$ fm$^{-1}$, $E/A \approx -16.72$ MeV. As to be expected, BHF calculation using only the two-body, especially using chiral N$^3$LO potential displays excessive attraction and is unable to produce saturation up to very high density. Thus, with only 2BF, the nonrelativistic BHF fails to obtain either the magnitude or the density near the empirical estimates (shown as rectangles) of the saturation property, thus, our results reconfirm the Coester *et al.* band [24]. The numerical values of saturation density $\rho$, binding energies per nucleon ($-E/A$), and other properties obtained in the present work, are given in Table 1.

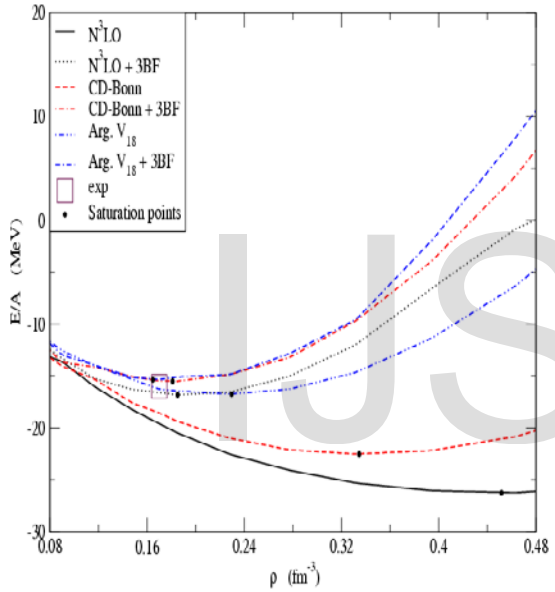


Fig. 2. $E/A$ in MeV for symmetric nuclear matter as a function of density using chiral N$^3$LO, CD-Bonn and Argonne $V_{18}$ potentials. The results are obtained using BHF approach with and without three-body force. For more details see the text.

As one expects, the qualitative features are confirmed in the subsequent implementation of the 3BF in BHF calculations of symmetric nuclear matter. The resulting EOS with 3BFs are shown in Fig. 2 and displayed by dotted line for chiral N$^3$LO+3BF, with dash-dotted line for CD-Bonn+3BF, and with dot-double dashed curve for $V_{18}$ + 3BF interactions. We note that the inclusion of 3BFs yields nuclear saturation very close to the empirical estimates (see also Table 1). More precisely, the saturation point for chiral N$^3$LO+3BF is $k_F \approx$ 1.4 fm$^{-1}$, $E/A \approx -16.8$ MeV, for the CD Bonn + 3BF is $k_F \approx 1.39$ fm$^{-1}$, $E/A \approx -15.5$ MeV, while for the V18 + 3BF interaction is $k_F \approx 1.36$ fm$^{-1}$, $E/A \approx -15.32$ MeV. One can see also, the main message coming from the comparisons explained in Fig. 2 is that the differences between the two EOS, which are apparent in the case without 3BF, are strongly reduced when 3BF are introduced. In the case of CD-Bonn+3BF and $V_{18}$ + 3BF interactions, their high density behavior is also similar, up to few times the saturation density. On the contrary, with the chiral N$^3$LO+3BF, one observes a quite different behavior than CD-Bonn+3BF and $V_{18}$ + 3BF interactions.

Table 1: The saturation points as a function of density, the incompressibility K and the symmetry energy at the saturation points for various potentials.

| Model | $\rho$ (fm$^{-3}$) | $k_F$ (fm$^{-1}$) | -E/A (MeV) | K (MeV) | $E_{sym}$ (MeV) |
|---|---|---|---|---|---|
| CD-Bonn +3BF | 0.180 | 1.386 | 15.497 | 179.26 | 26.033 |
| CD-Bonn | 0.331 | 1.698 | 22.505 | 265.88 | 35.363 |
| N$^3$LO + 3BF | 0.185 | 1.399 | 16.805 | 244.30 | 26.984 |
| N$^3$LO | 0.464 | 1.901 | 26.221 | 220.76 | 42.215 |
| Arg. $V_{18}$ +3BF | 0.169 | 1.358 | 15.319 | 482.48 | 24.814 |
| Arg. $V_{18}$ | 0.229 | 1.502 | 16.718 | 250.65 | 27.034 |

The resulting equation of state pure neutron matter, which is more appropriate for neutron star studies, is displayed in Fig. 3 with and without including 3BF. The solid and dotted lines represent the EOS for N$^3$LO, whereas the dash-dotted and dashed curves are for CD-Bonn. Finally, the dash-double dotted and dot-double dashed lines for $V_{18}$ potential.

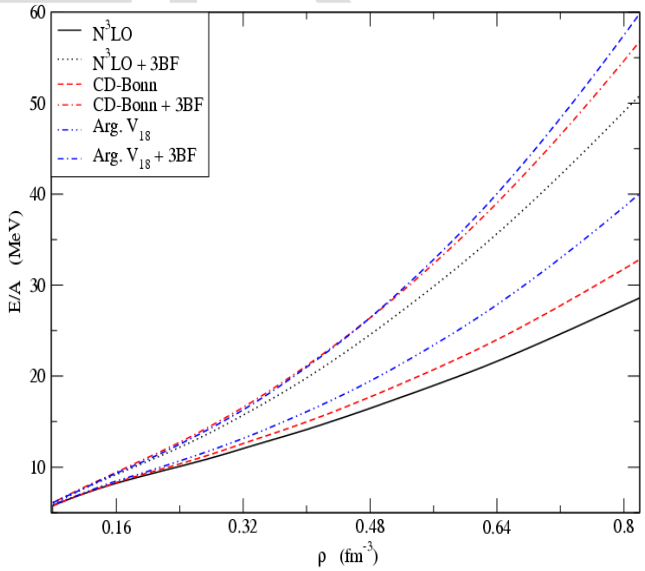


Fig. 3. $E/A$ in MeV for pure neutron matter as a function of density using chiral N$^3$LO, CD-Bonn and Argonne $V_{18}$ potentials. The results are obtained using BHF approach with and without three-body force. For more details see the text.

Moreover, the calculations are extended at densities up to about five times the saturation one. It appears from Fig. 3, the EOS of pure neutron matter given by $V_{18}$ potential is more repulsive, when phenomenological 3BF is included. Furthermore, the trend for the CD-Bonn potential is similar, especially at high densities. Whereas, the EOS, that is given by N$^3$LO interaction, is less repulsive than the other interactions.

### 3.3 Partial waves contribution to EOS

To see the effect and contributions of the 3BF in more details, we show, in figures 4 & 5, main partial wave decomposition of the calculated potential energy according to Eq. 5. If we look at partial waves depicted in Fig. 4, we see the attractive contribution in the $^3S_1$-$^3D_1$ channel, in the case of symmetric nuclear matter, is seen to increase by including the 2NF only, especially for chiral N$^3$LO and CD-Bonn, respectively.

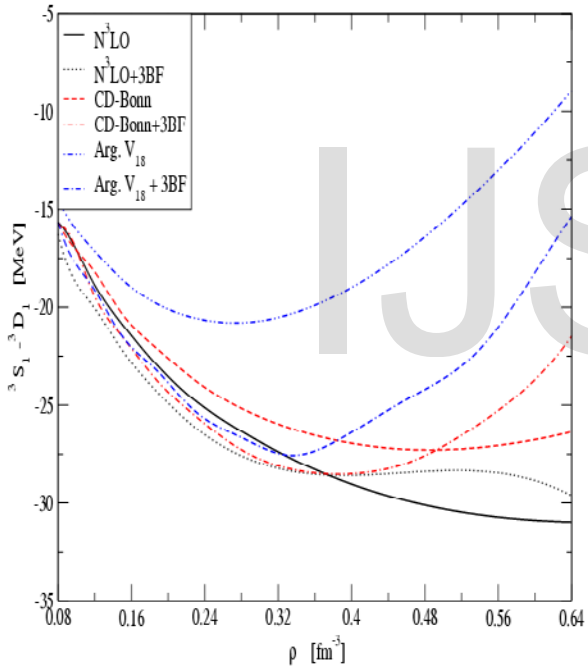


Fig. 4. The contribution from the $^3S_1$-$^3D_1$ partial wave in the contribution to the binding energy per nucleon of symmetric nuclear matter as a function of density ρ in fm$^{-3}$.

This means that the potential energy in the $^3S_1$-$^3D_1$ state turns out to be more attractive due to the enhancement of the tensor component. While in the case of Argonne $V_{18}$ potential, the resulting contribution represented by double dash-dotted line decreases as density increases. This behavior shifts the minimum of the energy to value close to the empirical one. This is due to the enhancement of the tensor correlation by the supplemented tensor force. In contrast, when the 3NF is included, there is significant change happen, especially for Argonne $V_{18}$ interaction, the 3BF induces a substantial repulsion as the density increases and there is a big difference observed between two cases. This means that the EOS becomes more repulsive as observed in Fig. 2. There is another contribution to EOS comes from $^1S_0$ channel, represented by left panel of Fig. 5. The same behavior is observed when the 3BF is included. Tables 2 & 3 shows the contribution of the most calculated partial waves to EOS of nuclear matter at $k_F$ = 1.35 fm-1 with and without 3BF.

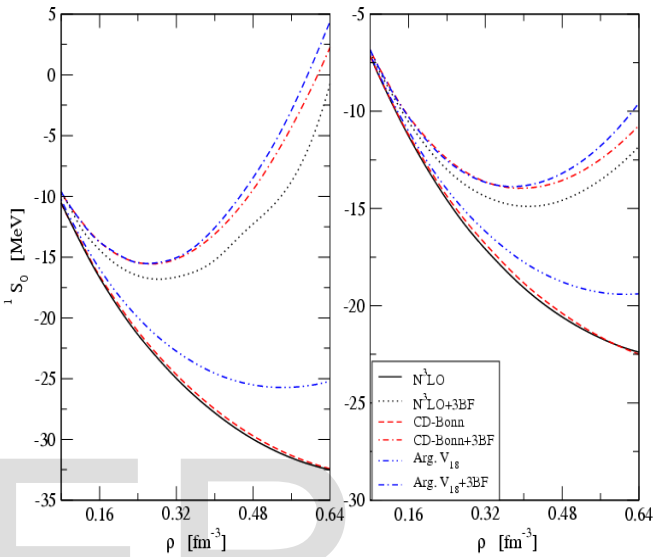


Fig. 5: The contribution from the $^1S_0$ partial wave in the contribution to the binding energy per nucleon is as a function of density ρ in fm$^{-3}$. Left panel is for symmetric nuclear matter, right panel is for pure neutron matter.

In the case of pure neutron matter, some partial waves are blocked in the antisymmetrization procedure of the two-neutron wave function, i.e. they can only be in total T = 1 isospin state. As expected from table III, the major change is observed in the $^1S_0$ partial wave, represented by right panel of Fig. 5. On the other hand, the $^1S_0$ contribution becomes less attractive as density increase. This makes EOS of pure nuclear matter more replies at high density. The other visible effect is in $^3P_2$ - $^3F_2$ mixing waves with negative values and the $^3P_1$ wave with positive values.

Table 2. Partial waves for symmetric nuclear matter for different potentials at $k_F$ = 1.35 fm$^{-1}$.

| | Argonne$V_{18}$ | | CD-Bonn | | N$^3$LO | |
|---|---|---|---|---|---|---|
| | BH+3BF | BHF | BHF+3BF | BHF | BHF+3BF | BHF |
| $^1S_0$ | -14.0591 | -16.396 | -13.9200 | -16.877 | -14.6086 | -17.073 |

| | | | | | | |
|---|---|---|---|---|---|---|
| $^3S_1$–$^3D_1$ | -22.3229 | -19.230 | -22.4899 | -20.931 | -22.8389 | -21.793 |
| $^3P_0$ | -3.1609 | -3.1727 | -3.2391 | -3.2556 | -3.2876 | -3.2920 |
| $^3P_1$ | 9.7969 | 9.3345 | 10.0816 | 9.6234 | 10.0289 | 9.5342 |
| $^1P_1$ | 4.4388 | 3.7671 | 4.4509 | 3.7782 | 4.4110 | 3.7903 |
| $^1D_2$ | -2.5796 | -2.5373 | -2.6363 | -2.6034 | -2.6131 | -2.5709 |
| $^3D_2$ | -3.3103 | -3.8561 | -3.3219 | -3.8595 | -3.3254 | -3.8849 |
| $^3P_2$-$^3F_2$ | -7.1974 | -7.7395 | -7.3331 | -7.9446 | -7.4039 | -8.1595 |
| $^1F_3$ | .5828 | .7721 | .5685 | .7578 | .6131 | .8021 |
| $^3F_3$ | .6101 | 1.2703 | .7355 | 1.3949 | .7158 | 1.3744 |
| $^1G_4$ | -.1694 | -.3812 | -.1917 | -.4037 | -.1924 | -.4044 |
| $^3G_4$ | -.1969 | -.6817 | -.1907 | -.6752 | -.1872 | -.6721 |
| $^3D_3$-$^3G_3$ | -.3982 | .1035 | -.3604 | .1317 | -.1375 | .3048 |
| $^3F_4$-$^3H_4$ | -.0991 | -.3821 | -.1619 | -.4461 | -.1017 | -.3872 |
| $^3G_5$-$^3I_5$ | -.0504 | .0954 | -.0527 | .0933 | -.0343 | .1114 |
| $^1H_5$ | .0322 | .1928 | .0325 | .1931 | .03534 | .1959 |
| $^3H_5$ | -.0414 | .2673 | -.0141 | .2946 | -.0103 | .2984 |
| $^1I_6$ | .0213 | -.0849 | .0107 | -.0956 | .0094 | -.0969 |
| $^3I_6$ | .0371 | -.1483 | .0369 | -.1484 | .0361 | -.1493 |
| $^3H_6$-$^3L_6$ | .0437 | -.0361 | .0297 | -.0502 | .0292 | -.0506 |
| $^1J_7$ | -.0161 | .0489 | -.0144 | .0507 | -.0140 | .0511 |
| $^3J_7$ | -.0479 | .0587 | -.0371 | .0695 | -.0365 | .0701 |
| $^3J_7$-$^3K_7$ | -.0205 | .0212 | -.0199 | .0218 | -.0195 | .0222 |
| $^1K_8$ | .0176 | -.0201 | .0126 | -.0250 | .0123 | -.0253 |
| $^3J_8$-$^3L_8$ | .0152 | -.0067 | .0122 | -.0097 | .0121 | -.0099 |
| $^3K_8$ | .0247 | -.0345 | .0227 | -.0366 | .0224 | -.0368 |
| $^1L_9$ | -.0086 | .0120 | -.0068 | .0138 | -.0067 | .0139 |
| $^3K_9$-$^3M_9$ | -.0068 | .0045 | -.0065 | .0048 | -.0064 | .0049 |
| $^3L_9$ | -.0186 | .0129 | -.0141 | .0175 | -.0139 | **.0177** |

Table 3. Partial waves for pure neutron matter for different potentials at $k_F$ = 1.35 fm$^{-1}$.

| | Argonne $V_{18}$ | | CD-Bonn | | $N^3LO$ | |
|---|---|---|---|---|---|---|
| | BHF+3BF | BHF | BHF+3BF | BHF+3BF | BHF | BHF+3BF |
| $^1S_0$ | -10.531 | -11.286 | -10.40 | -11.39 | -10.79 | -11.56 |
| $^3P_0$ | -2.3446 | -2.3488 | -2.309 | -2.316 | -2.302 | -2.305 |
| $^3P_1$ | 6.4506 | 6.3114 | 6.5221 | 6.3771 | 6.5112 | 6.3644 |
| $^1D_2$ | -1.8000 | -1.7852 | -1.784 | -1.773 | -1.762 | -1.747 |
| $^3P_2$-$^3F_2$ | -5.3761 | -5.5267 | -5.402 | -5.580 | -5.409 | -5.638 |
| $^3F_3$ | .7449 | .9651 | .7685 | .9884 | .7513 | .9709 |
| $^1G_4$ | -.2194 | -.2899 | -.2161 | -.2867 | -.2153 | -.2859 |
| $^3F_4$-$^3H_4$ | -.1994 | -.2939 | -.2227 | -.3177 | -.1811 | -.2765 |
| $^3H_5$ | .1153 | .2182 | .1137 | .2166 | .1151 | .2180 |
| $^1I_6$ | -.0349 | -.0703 | -.0354 | -.0708 | -.0359 | -.0713 |
| $^3H_6$-$^3L_6$ | -.0065 | -.0332 | -.0114 | -.0380 | -.0114 | -.0381 |
| $^3J_7$ | .0160 | .0516 | .0174 | .0529 | .0175 | .0530 |
| $^1K_8$ | -.0053 | -.0179 | -.0067 | -.0193 | -.0068 | -.0193 |
| $^3J_8$-$^3L_8$ | .0006 | -.0067 | -.0004 | -.0077 | -.0004 | -.0077 |
| $^3L_9$ | .0016 | .0122 | .0033 | .0139 | .0033 | .0139 |

### 3.4 Incompressibility K and Symmetry energy $a_s$

There is another important characteristic of the EOS and it enters in the discussion of a variety of phenomena such as supernovae explosions or heavy ion collisions, that it is the incompressibility K. It measures the stiffness of the EOS, usually calculated at saturation point:

$$K = k_F^2 \frac{\partial P(\rho)}{\partial k_F^2}\Big|_{k=k_F^0} = 9\rho^2 \frac{\partial^2 E/A(\rho)}{\partial \rho^2}\Big|_{\rho=\rho_0} \quad (10)$$

The experimental value of the incompressibility of symmetric nuclear matter at its saturation density $\rho_0$ has been determined to be 230 ± 40 MeV [25]. At the saturation density, the values of the incompressibility obtained for symmetric nuclear matter are summarized in table 1. As one sees, the values of incompressibility K are compatible with the experimental value.

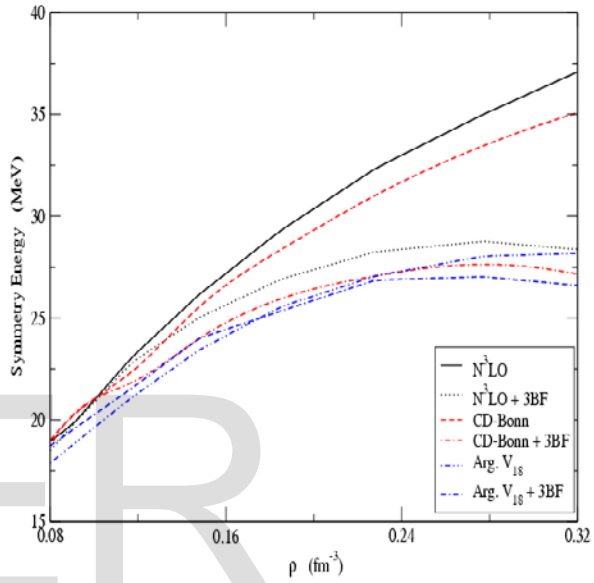


Fig. 6: The symmetry energy obtained from Eq. (12) as a function of the density ρ in fm$^{-3}$.

The EOS of PNM combined with that of SNM provides us with information on the iso-spin effects [26], in particular on the symmetry energy $a_s$. The symmetry energy of nuclear matter is defined as a second derivative of energy per nucleon $E/A$ with respect to the asymmetry parameter $a$ as follows

$$a_s(\rho, \alpha) = \frac{1}{2}\left[\frac{\delta^2 E/A(\rho,\alpha)}{\delta \alpha^2}\right]\Big|_{\rho=\rho_0} \quad (11)$$

where we introduce the asymmetry parameter $a = (\rho_n - \rho_p)/\rho$. Both $\rho_n$ and $\rho_p$ are the neutron and proton densities in asymmetric nuclear matter and $\rho_n + \rho_p = \rho$ is the total density of asymmetric nuclear matter. It is well established [27, 28] that the binding energy per nucleon $E/A$ fulfills the simple $\alpha^2$-law, $a_s$. $a^2 = E/A\ (\rho, a=1) - E/A(\rho, a = 0)$, not only for $a \leq 1$, as assumed in the empirical nuclear mass formula [29], but also in the whole asymmetry range and the behavior is linear. This enables us to calculate the symmetry energy $as$ in terms of the difference between the binding energy of pure neutron matter $E/A\ (\rho, a=1)$ and that of symmetric nuclear

matter $E/A\ (\rho,a=0)$, i.e.

$$a_s = E/A\ (\rho,\alpha=1) - E/A(\rho,\alpha=0), \quad (12)$$

but one would refrain from applying it at very high density. Fig. 6 shows the values of the s ymmetry energy for the different EOSs that we consider, namely, the nonrelativistic BHF calculations with the chiral N$^3$LO, CD-Bonn and the Argonne V18 potentials with and without three-body forces. The values of symmetry energy according to Eq. 12 at saturation points are found to be 26.98, 26.03 and 24.5 MeV for N$^3$LO+3BF, CD-Bonn+3BF and $V_{18}$ +3BF potentials as they be tabulated in table I, respectively. These values close to the empirical value, as = 30 ± 2 MeV.

## 4 Conclusion

We have presented results for both microscopic and macroscopic properties of infinite nuclear matter in the frame of BHF theory. The calculations have performed with a variety of interactions. These include phase-shift equivalent forces with strong and soft short-range cores. These interactions are chiral N$^3$LO, CD-Bonn and Argonne $V_{18}$ potentials. The single-particle potential is analyzed at saturation density using different potentials with and without three-body force. Main differences were noticed at zero momentum, i.e. depth of the single-particle potential. Also, we observed a visible repulsive effect provided by 3BF for all momenta. There is another behavior of single-particle potentials which show a significant deviation from a parabolic shape in particular at momentum slightly above the Fermi momentum kF when the exact treatment of Pauli's operator is chosen.
The calculation of the SNM's and PNM's EOS has been performed within BHF theory using 2BF and 3BF. It is found that, in the case of SNM, the EOS is strongly over bound using only the N$^3$LO 2BF in the BHF approach compared to other interactions. Both the CD Bonn and $V_{18}$ give a quite different saturation point and overall EOS, but the introduction of the same 3BF shifts both EOS towards each other and close to phenomenology. On the contrary, this behavior is different when the results are done using the chiral N$^3$LO plus 3BF. The bulk properties of infinite nuclear matter close to the empirical values when the 3BF is included to BHF approach.

## References

[1] H. Müther and A. Polls, Progress in Particle and Nuclear Physics, vol.45, 243-334 (2000).
[2] M. Baldo, "Nuclear Methods and the Nuclear Equation of State", (World Scientific, Singapore, 1999).
[3] J. Carlson, V.R. Pandharipande, and R.B. Wiringa, Nucl. Phys. A 401, 59 (1983).
[4] A. Akmal, V.R. Pandharipande, and D.G. Ravenhall, Phys. Rev. C 58, 1804 (1998);
[5] B.S. Pudliner, V. R. Pandharipande, J. Carlson, S.C. Pieper, and R.B. Wiringa, Phys. Rev. C 56, 1720 (1997).
[6] J. Carlson and R. Schiavilla, Rev. Mod. Phys. 70, 743 (1998)
[7] W.H. Dickhoff and C. Barbieri, "Self-consistent Green's function method for nuclei and nuclear matter," Progress in Particle and Nuclear Physics, vol. 52, no. 2, pp. 377–496, 2004
[8] Khaled Hassaneen and Hesham Mansour, "THE PROPERTIES OF NUCLEAR MATTER ", Phys. Int. 4 (1), 37-59 (2013), doi:10.3844/pisp.2013.37.59
[9] F. Coester, S. Cohen, B.D. Day, C.M. Vincent, Phys. Rev. C 1 (1970) 769.
[10] Kh.S.A. Hassaneen, H. M. Abo-Elsebaa, E. A. Sultan, and H. M. M. Mansour, "Nuclear binding energy and symmetry energy of nuclear matter with modern nucleon-nucleon potentials," Annals of Physics, 326, 566–577, (2011).
[11] P. Gögelein, E.N.E. van Dalen, Kh. Gad, Kh.S.A. Hassaneen, and H. Müther, Phys. Rev. C79, 024308 (2009).
[12] R. Brockmann and R. Machleidt, Phys. Rev. C 42, 1965 (1990).
[13] D. R. Entem and R. Machleidt, Phys. Rev. C 68, 041001 (2003).
[14] A. Ekström, G. Baardsen, C. Forssén, G. Hagen, M. Hjorth-Jensen, G. R. Jansen, R. Machleidt, W. Nazarewicz, T. Papenbrock, J. Sarich, et al., Phys. Rev. Lett. 110, 192502 (2013).
[15] R. Machleidt, Phys. Rev. C 63: 024001, (2001).
[16] R. B. Wiringa, V. G. J. Stoks, and R. Schiavilla, Phys. Rev. C 51, 38 (1995).
[17] M. Kohno, Phys. Rev. C88, 064005 (2013).
[18] E. Epelbaum, W. Göckle, and U.-G. Meißner, Nucl. Phys. A747, 362 (2005).
[19] J. Carlson, V.R. Pandharipande, and R.B. Wiringa, Nucl. Phys. A 401, 59 (1983).
[20] J. P. Jeukenne, A. Lejeune, and C. Mahaux, Phys. Rep. 25, 83 (1976).
[21] E. Schiller, H. Müther and P. Czerski, Phys. Rev. C 59, 2934 (1999) and C 60, 059901(E) (1999).
[22] M. Baldo and Alaa Eldeen Shaban, Phys. Lett. B 661, 373 (2008).
[23] H. M. M. Mansour and Kh.S.A. Hassaneen, "The Properties of Nuclear Matter at Zero and Finite Temperature" Physics of Atomic Nuclei, Vol. 77, No. 3, pp. 290–298, (2014).
[24] F. Coester, S. Cohen, B. Day, and C. M. Vincent, Phys. Rev. C 1, 769 (1970).
[25] J.R. Stone, N.J. Stone, and S.A. Moszkowski, Phys. Rev. C89, 044316. (2013).
[26] W. Zuo, I. Bombaci and U. Lombardo, Phys. Rev. C60, 024605 (1999).
[27] Kh. Gad and Kh.S.A. Hassaneen, Nucl. Phys. A793, 67-78 (2007).
[28] Kh.S.A. Hassaneen and Kh. Gad, J. Phys. Soc. Jpn 77, 084201 (2008).
[29] P. E. Haustein, Atomic Data and Nuclear Data Tables 39, 185 (1988).